DISCRETE AND CONTINUOUS
DYNAMICAL SYSTEMS SERIES B
Volume **21**, Number **8**, October **2016**

doi:10.3934/dcdsb.2016061

pp. **2567–2585**

A REACTION DIFFUSION SYSTEM MODELING VIRUS DYNAMICS AND CTLS RESPONSE WITH CHEMOTAXIS

Xiulan Lai*

Institute for Mathematical Sciences, Renmin University of China
Beijing 100872, China

Xingfu Zou

Department of Applied Mathematics, University of Western Ontario
London, Ontario, N6A 5B7, Canada
and
School of Mathematics and Statistics, Central South University
Changsha 410083, Hunan, China

(Communicated by the Yuan Lou)

Abstract. In this paper, we study the effect of chemotactic movement of CTLs on HIV-1 infection dynamics by a reaction diffusion system with chemotaxis. Choosing a typical chemosensitive function, we find that *chemoattractive* movement of CTLs due to HIV infection does not change stability of a positive steady state of the model, meaning that the stability/instability of the model remains the same as in the model without spatial effect. However, *chemorepulsion* movement of CTLs can destabilize the positive steady state as the strength of the chemotactic sensitivity increases. In this case, Turing instability occurs, which may result in Hopf bifurcation or steady state bifurcation, and spatial inhomogeneous pattern forms.

1. **Introduction.** Some living organisms or cells, such as somatic cells and lymphocytes, have the ability to detect certain chemicals in their environment and adapt their movement accordingly, moving either toward or away from the chemical stimulus. This phenomenon is called *chemotaxis* or generally *chemosensitive movement*. In the mathematical literature, the term *chemotaxis* is used broadly to describe general chemosensitive movement responses, including chemoattraction (positive chemotaxis) and chemorepulsion (negative chemotaxis). However, in the experimental community, for example, in leukocytes trafficking mechanism, the term *chemotaxis* is defined only as chemoattraction, that is, an active movement of leukocytes toward chemokinetic agents, while chemorepulsion is referred to as *fugetaxis*, describing the active movement of leukocytes away from chemokinetic agents. In

2010 *Mathematics Subject Classification.* Primary: 35K57, 92C17; Secondary: 35B35, 35B36, 35B38, 92C37.

Key words and phrases. HIV-1 infection, CTLs, chemoattraction, chemorepulsion, reaction diffusion equation.

The research is supported by the Fundamental Research Funds for the Central Universities, and the Research Funds of Renmin University of China, CSC Overseas Doctoral Scholarship (China) and NSERC (Canada).

* Corresponding author: Xiulan Lai.

this paper, we use *chemotaxis* to mean the general chemosensitive movement, either chemoattraction (positive chemotaxis) or chemorepulsion (positive chemotaxis).

Cytotoxic T lymphocytes (CTLs), or effector $CD8^+$ T cells, play a critical role in host defense against human immunodeficiency virus type 1 (HIV-1) infection. Normally, effector T cells leave lymph nodes and traffic to peripheral sites of infection. However, in HIV-1 infection, the majority of HIV-1 replication occurs in lymphoid tissues. To implement their antiviral activity, CTLs must migrate reversely back into infected lymphoid tissues, and remain within them . Thus the recruitment of CTLs is very important for the clearance of HIV-1. The movement of lymphocytes between the circulatory system and specific tissues is coordinated by Chemokines and their receptors. For example, inflammatory chemokines guide effector T cells to exit lymphoid tissues and home to peripheral sites of infection. HIV-1 infection and replication in the lymphoid tissues changes the chemotactic and cellular environments. As HIV-1 disease progresses, the homing ability of CTLs to infected lymph nodes may be disrupted, due either to reduced lymph node chemokine levels or reduced CTLs chemokine receptor expression, and thus affect the cytotoxic effect of CTLs in advanced HIV-1 infection [5].

Many viruses encode chemotactically active proteins. For instance, the envelope protein gp120 of HIV-1 has been shown to act as a T-cell chemoattractant via binding to the chemokine receptor and HIV-1 coreceptor CXCR4. However, some studies [4, 18] showed that HIV-specific CTLs move toward or away from the CXCR4-binding HIV-1 gp120 in a concentration-dependent manner. The high concentration of CXCR4-binding HIV-1 gp120 repels HIV-specific CTLs, while low concentration of gp120 attracts CTLs with specific interaction with CXCR4. The repellant activity of HIV-1 gp120 on CTLs causes the active movement of HIV-1-specific CTLs away from the site of infection, which allows the virus to evade immune recognition and invade immune system.

In this paper, we study the effect of chemotactic movement of CTLs during HIV-1 infection by mathematical modeling. We denote by $T(x,t)$, $I(x,t)$ and $E(x,t)$ the population densities of uninfected $CD4^+$ T cells, infected $CD4^+$ T cells and CTLs at location x at time t respectively. Assuming that the virus population is at a quasi-steady state [15], we consider the following model.

$$\begin{aligned}
\frac{\partial T}{\partial t} &= D_T \Delta T + h - d_T T - \beta T I,\\
\frac{\partial I}{\partial t} &= D_I \Delta I + \beta T I - d_I I - pIE,\\
\frac{\partial E}{\partial t} &= D_E \Delta E + \nabla \cdot [E\Psi(E,I)\nabla I] + \frac{cEI}{1+\eta E} - d_E E.
\end{aligned} \tag{1}$$

Here, we assume that uninfected $CD4^+$ T cells are recruited at a constant rate h, and infected at a rate βTI. The infected cells are cleared by CTLs at a rate pIE. The CTLs proliferate in response to antigenic simulation with a rate cEI, and the rate of CTLs expansion saturates as the number of CTLs grows to relatively high numbers. $1/\eta$ represents the saturation level. Uninfected $CD4^+$ T cells, infected $CD4^+$ T cells and CTLs are lost at rates $d_T T$, $d_I I$ and $d_E E$ respectively.

In this model, we assume that uninfected $CD4^+$ T cells and infected $CD4^+$ T cells move randomly, with the diffusion coefficients D_T and D_I respectively. In contrast, the diffusion of CTLs consists of two parts, the random diffusion and the chemotactic movement. The random diffusion coefficient is assumed to be D_E, that is,

the diffusion flux of CTLs is proportional to their density gradient $\mathbf{J}_D = -D_E \nabla E$. As mentioned above, the HIV-1 viral protein gp120, binding with the coreceptor CXCR4, acts as a chemoattractant or chemorepellant for CTLs. Thus, the chemotaxis flux $\mathbf{J}_C$ of CTLs depends on the their own density, the density of HIV-1 viral protein gp120, and the density gradient of this protein. Here we assume that the density of viral protein gp120 binding to CXCR4 is proportional to the density of infected $CD4^+$ T cells, and the chemotaxis flux of CTLs is $\mathbf{J}_C = -E\Psi(E, I)\nabla I$. The derivation of this chemotactic term can be referred from the works of Painter [12] and Hillen [8]. The function $\Psi(E, I)$ represents the chemotactic response, which denotes chemoattraction (chemorepulsion) if it is negative (positive). Notice that movement of $CD4^+$ T cells may be very slow comparing with CTLs, that is, $D_T \ll D_E$, or they even do not diffuse at all in the lymphoid tissue. Here we assume that $D_T > 0$ but very small compared with D_E for the sake of mathematical consideration.

For the PDE model system (1), we consider the no-flux boundary conditions:

$$\frac{\partial T}{\partial \nu} = \frac{\partial I}{\partial \nu} = \frac{\partial E}{\partial \nu} = 0, \quad \forall x \in \partial\Omega, \quad t > 0. \tag{2}$$

The rest of the paper is organized as follows. In section 2 we discuss the well-posedness of the model. Linear stability of the steady states are shown in section 3. The conditions for Turing instability and pattern formation are derived in section 4. Numerical simulation about the stability of positive steady state, steady state bifurcation, Hopf bifurcation and pattern formation are shown in section 5. Finally, we present conclusions and discussions in section 6.

2. **Global existence of solutions.** We assume that Ω is a bounded domain in $\mathbb{R}^n$ with smooth boundary $\partial\Omega$. For the chemosensitive function $\Psi(E, I)$, we post the following standard hypothesis:

(H) $\Psi \in C^2(\mathbb{R}^2_+, \mathbb{R}_+)$, satisfying (i) $\Psi(0, I) = 0$, $\Psi(E, 0)=0$; (ii) there exists sufficiently large $E_M > 0$, such that $\Psi(E, I) = 0$, for $E \geq E_M$; (iii) for chemorepulsion case $\Psi(E, I) > 0$ for $0 < E < E_M$, and for chemoattractive case $\Psi(E, I) < 0$ for $0 < E < E_M$.

Let $\rho > n$ so that the space $\mathbf{W}^{1,\rho}(\Omega, \mathbb{R}^3)$ is continuously embedded into the continuous function space $\mathbf{C}(\Omega, \mathbb{R}^3)$ (see, e.g.,[1]). We consider solutions of (1)-(2) in the following solution space

$$\mathbf{X} := \left\{ w \in \mathbf{W}^{1,\rho}(\Omega, \mathbb{R}^3) \mid w(\bar{\Omega}) \in \mathbb{R}^3_+, \ \frac{\partial w}{\partial \nu} = 0 \text{ on } \partial\Omega \right\}.$$

System (1)-(2) can be rewritten as the following abstract quasilinear parabolic problem

$$\begin{cases} w_t + \mathcal{A}(w)w = \mathcal{F}(w), \\ \mathcal{B}w = 0, \end{cases} \tag{3}$$

where for $z = (z_1, z_2, z_3)$

$$\mathcal{A}(z)w = -\sum_{j,k=1}^{n} \partial_j(a_{jk}(z)\partial_k w), \ \mathcal{B}w = \frac{\partial w}{\partial \nu},$$

$$a(z) = (a_{j,k}(z))_{3\times 3} = \begin{pmatrix} D_T & 0 & 0 \\ 0 & D_T & 0 \\ 0 & z_3\Psi(z_3, z_2) & D_E \end{pmatrix},$$

and for $w = (T, I, E)$,

$$\mathcal{F}(w) = \left(h - d_T T - \beta T I, \beta T I - d_I I - pIE, \frac{cEI}{1+\eta E} - d_E E \right)^{\mathsf{T}}.$$

We see that $a(z) \in \mathbf{C}^2(\mathbb{R}^3_+, \mathcal{L}(\mathbb{R}^3))$, where $\mathcal{L}(\mathbb{R}^3)$ denote the space of all 3×3 real matrices, and the eigenvalues of $a(z)$ are all positive for each $z \in \mathbb{R}^3_+$. Moreover, the boundary value problem $(\mathcal{A}, \mathcal{B})$ is normally elliptic (see, e.g., [3]).

We consider (1)-(2) with the following initial conditions

$$\begin{cases} T(0,x) = T_0(x) \geq 0, \quad I(0,x) = I_0(x) \geq 0, \quad E(0,x) = E_0(x) \geq 0, \\ \text{with } (T_0(x), I_0(x), E_0(x)) \in C(\bar{\Omega}, R^3_+). \end{cases} \tag{4}$$

Existence and uniqueness, as well as nonnegativity of solution of (1)-(2) are obtained in the following two theorems.

Theorem 2.1. *The following statements hold:*

(i) The problem (1)-(2) has a unique solution (T, I, E) with

$$(T, I, E) \in \mathbf{C}([0, \tau_0), \mathbf{X}) \cap \mathbf{C}^{2,1}((0, \tau_0) \times \bar{\Omega}, \mathbb{R}^3),$$

defined on a maximal interval $[0, \tau_0) \times \Omega$ where τ_0 depends on the initial data (T_0, I_0, E_0);

(ii) $T(t,x) \geq 0$, $I(t,x) \geq 0$, $E(t,x) \geq 0$, for all $(t,x) \in [0, \tau_0) \times \Omega$;

(iii) If $(T, I, E)|_{([0,\tau_0)\cap[0,\tau])}$ is bounded in $\mathbf{C}(\bar{\Omega}, \mathbb{R}^3)$ and bounded away from the boundary of $\mathbb{R}^3_+$ for evrey $\tau > 0$, then $\tau_0 = +\infty$, namely, the solution exists globally.

Proof. Noting that System (3) is normal eliptic and triangular, (i) follows from Amann [2](Theorem 1) or Amann [3] (Theorem 14.4 and Theorem 14.6). From Amann [3] (Theorem 15.1), we get (ii), the nonegativity of the solution. Apply Amann [2] (Theorem 5.2) , we obtain (iii), the condition for global existence of a solution. □

The following theorem confirms that the existence of solution is indeed global if $D_T = D_I$.

Theorem 2.2. *Assume that $D_T = D_I$. Suppose that (T, I, E) is the solution obtained in Theorem 1, then it is a global solution to system (1).*

Proof. In order to prove the global existence of the solution, by (ii) and (iii) of Theorem 1, we only need to prove that (T, I, E) is bounded from above.

From the T and I equations of (1), we see that

$$\begin{aligned} \frac{\partial}{\partial t}(T + I) &= D_T \Delta (T + I) + h - d_T T - d_I I - pIE \\ &\leq D_T \Delta (T + I) + h - d_m (T + I), \end{aligned}$$

where $d_m = \min\{d_T, d_{T^*}\}$. By Lemma 1 in Lou and Zhao [9], $\bar{h}/d_m$ is globally attractive in $\mathbf{C}(\bar{\Omega}, \mathbb{R})$ for the scalar parabolic equation

$$\begin{aligned} \frac{\partial w(t,x)}{\partial t} &= D_T \Delta w(t,x) + h - d_m w(t,x), \ x \in \Omega, \ t > 0, \\ \frac{\partial w}{\partial \nu} &= 0, \ x \in \partial\Omega, \ t > 0. \end{aligned}$$

The parabolic comparison theorem (see, e.g., Theorem 7.3.4 in [13]) implies that $T+I$ is bounded on $[0,\tau)$. This together with the non-negativity of $T(t,x)$ and $I(t,x)$ further implies that $T(t,x)$ and $I(t,x)$ are both bounded. We assume $0 \le T(t,x) \le T_M$, $0 \le I(t,x) \le I_M$.

Let $E_M = \frac{c}{\eta d_E} I_M$. Define the differential operator $\mathcal{P}$ by

$$\mathcal{P}E = E_t - D_E \Delta E - \nabla \cdot (E\Psi(E,I)\nabla I) + \left(d_E E - \frac{cEI}{1+\eta E} \right).$$

For any solution of system (1), we have $\mathcal{P}E = 0$. However, for $E_M = \frac{c}{\eta d_E} I_M$ sufficiently large, by (H), we have

$$\mathcal{P}E_M = d_E E_M - \frac{cE_M I}{1+\eta E_M} \ge d_E E_M - \frac{c}{\eta} I_M = 0.$$

On the boundary $\partial\Omega$, $\frac{\partial E_M}{\partial \nu} = 0$. Therefore, $E = E_M$ is a upper solution of the E equation in system (1). By the comparison principle, we then obtain that $E(t,x) \le E_M$. Therefore, the solution (T,I,E) is bounded from above, completing the proof. □

Notice that we assumed $D_T = D_I$ in the proof of Theorem 2, and this will be assumed in what follows.

3. **Linear stability analysis.** System (1) has three possible spatially homogeneous steady states:

(i) the infection-free steady state $S_0 = (h/d_T, 0, 0)$ always exists;

(ii) if $\mathcal{R}_0 := h\beta/d_I d_T > 1$, there exists a virus-established steady state $S_1 = (T_1, I_1, 0)$, where

$$T_1 = \frac{d_I}{\beta}, \quad I_1 = \frac{h}{d_I} - \frac{d_T}{\beta};$$

(iii) if $cI_1 > d_E$, which is equivalent to $\mathcal{R}_0 > 1 + \beta d_E / c d_T$, there exists a positive steady state $S^* = (T^*, I^*, E^*)$, where

$$T^* = \frac{1}{2\beta}\left[-\left(\frac{d_T cp}{\beta d_E \eta} + \frac{p}{\eta} - d_I \right) + \sqrt{\left(\frac{d_T cp}{\beta d_E \eta} + \frac{p}{\eta} - d_I \right)^2 + 4h\frac{cp}{d_E \eta}} \right]$$

$$I^* = \frac{h}{\beta T^*} - \frac{d_T}{\beta}, \quad E^* = \frac{1}{p}(\beta T^* - d_I).$$

Notice that if there is no saturation of CTL, that is $\eta \to 0$, the positive steady state tends to $S_0^* = (T_0^*, I_0^*, E_0^*)$ where

$$T_0^* = \frac{hc}{d_T c + \beta d_E}, \quad I_0^* = \frac{d_E}{c}, \quad E_0^* = \frac{1}{p}(\beta T^* - d_I).$$

It can be verified that under the assumption $cI_1 > d_E$, the following holds

$$I_0^* < I^* < I_1.$$

Indeed,

$$\begin{aligned} I^* < I_1 &\iff \beta T^* > d_I \\ &\iff \left(\frac{d_T cp}{\beta d_E \eta} + \frac{p}{\eta} - d_I \right)^2 + 4h\frac{cp}{d_E \eta} > \left(\frac{d_T cp}{\beta d_E \eta} + \frac{p}{\eta} + d_I \right)^2 \end{aligned}$$

$$\begin{aligned}
&\iff \quad 4h\frac{cp}{d_E\eta} > 4d_I\left(\frac{d_Tcp}{\beta d_E\eta}+\frac{p}{\eta}\right)\\
&\iff \quad \frac{h}{d_I} > \frac{d_T}{\beta}+\frac{d_E}{c}\\
&\iff \quad cI_1 > d_E.
\end{aligned}$$

$$\begin{aligned}
I_0^* < I^* \quad &\iff \quad \beta T^* < \frac{hc\beta}{d_Tc+d_E\beta}\\
&\iff \quad \left(\frac{d_Tcp}{\beta d_E\eta}+\frac{p}{\eta}-d_I\right)^2+4h\frac{cp}{d_E\eta}\\
&\qquad\quad < \left[\frac{2hc\beta}{d_Tc+d_E\beta}+\left(\frac{d_Tcp}{\beta d_E\eta}+\frac{p}{\eta}-d_I\right)\right]^2\\
&\iff \quad 4h\frac{cp}{d_E\eta} < \left(\frac{2hc\beta}{d_Tc+d_E\beta}\right)^2+\frac{4hc\beta}{d_Tc+d_E\beta}\left(\frac{d_Tcp}{\beta d_E\eta}+\frac{p}{\eta}-d_I\right)\\
&\iff \quad \frac{p(d_Tc+d_E\beta)}{\beta d_E\eta} < \frac{hc\beta}{d_Tc+d_E\beta}+\frac{d_Tcp}{\beta d_E\eta}+\frac{p}{\eta}-d_I\\
&\iff \quad \frac{hc\beta}{d_Tc+d_E\beta}-d_I>0\\
&\iff \quad cI_1 > d_E.
\end{aligned}$$

It is straightforward to verify that $cI_1 > d_E$ is equivalent to

$$\mathcal{R}_0 > 1+\frac{\beta d_E}{cd_T}.$$

The formulas of the positive steady state (T^*, I^*, E^*) are very complex. Before discussing the stability of the steady states, we investigate the dependence of the positive steady state on parameters. One can easily verify that T^* is an increasing function of p, c, d_I, and a decreasing function of β, η, d_T, d_E; I^* is an increasing function of β, η, d_E, and a decreasing function of p, c, d_T, d_I; E^* is an increasing function of c, and a decreasing function of η, d_E. Here, we take the parameter c as an examples to demonstrate that as c increases, T^* and E^* increases while I^* decreases.

For $c>0$, let $f(c) := \frac{d_Tcp}{\beta d_E\eta}+\frac{p}{\eta}-d_I$, $g(c) := 4h\frac{cp}{d_E\eta}$, and $\mathcal{F}(c) := -f(c)+\sqrt{f(c)^2+g(c)}$, then $T^*(c) = \frac{1}{2\beta}\mathcal{F}(c)$, and

$$\mathcal{F}'(c) = -f'(c)+\frac{2f(c)f'(c)+g'(c)}{2\sqrt{f(c)^2+g(c)}} = \frac{f'(c)}{\sqrt{f(c)^2+g(c)}}\left[\frac{g'(c)}{2f'(c)}-\mathcal{F}(c)\right].$$

Furthermore,

$$f'(c) = \frac{d_Tp}{\beta d_E\eta}, \quad g'(c) = 4h\frac{p}{d_E\eta}, \quad \mathcal{F}'(c) = \frac{2\beta f'(c)}{\sqrt{f(c)^2+g(c)}}\left[\frac{h}{d_T}-T^*\right]>0.$$

Therefore,

$$T^{*\prime}(c) = \frac{1}{2\beta}\mathcal{F}'(c)>0, \quad I^{*\prime}(c) = -\frac{hT^{*\prime}(c)}{\beta T^*(c)^2}<0, \quad E^{*\prime}(c) = \frac{\beta}{p}T^{*\prime}(c)>0.$$

In a similar way, we can show the dependence of T^*, I^* and E^* on other parameters.

In what follows, we discuss the linear stability of the steady states. In the absence of spatial effect, we know that S_0 is locally asymptotically stable if $\mathcal{R}_0<1$; S_1 is

locally asymptotically stable if $\mathcal{R}_0 > 1$ and $cI_1 < d_E$; S^* is locally asymptotically stable if $cI_1 > d_E$. In fact, these results can be obtained from the discussion below as a special case when the spatial effect disappears.

Let $\hat{S} = (\hat{T}, \hat{I}, \hat{E})$ be a steady state of the system (1). Then the linearization of system (1) at $\hat{S}$ is given by

$$\frac{\partial u}{\partial t} = (\mathrm{D}\Delta + \mathrm{A})u, \tag{5}$$

where

$$\mathrm{D}(\hat{S}) = \begin{pmatrix} D_T & 0 & 0 \\ 0 & D_T & 0 \\ 0 & \hat{\Psi} & D_E \end{pmatrix}, \ \mathrm{A}(\hat{S}) = \begin{pmatrix} -d_T - \beta\hat{I} & -\beta\hat{T} & 0 \\ \beta\hat{I} & \beta\hat{T} - d_I - p\hat{E} & -p\hat{I} \\ 0 & \frac{c\hat{E}}{1+\eta\hat{E}} & \frac{c\hat{I}}{(1+\eta\hat{E})^2} - d_E \end{pmatrix},$$

and $u = (u_1, u_2, u_3, u_4)^T$, $\hat{\Psi}(\hat{S}) := \hat{E}\Psi(\hat{E}, \hat{I})$. Notice that $\hat{\Psi}(S_0) = 0$, $\hat{\Psi}(S_1) = 0$ and $\Psi^* := \hat{\Psi}(S^*) = E^*\Psi(E^*, I^*)$.

The corresponding characteristic polynomial of the linearized system (5) is

$$| \lambda I + \mathrm{D}k^2 - \mathrm{A} | = 0, \tag{6}$$

where $k \geq 0$, called the wavenumbers or the wave modes, are the eigenvalues of Laplace operator on a finite domain with no-flux boundary conditions. For instance, in one-dimensional domain $[0, L]$, $k^2 = n^2L^2/\pi^2$, or in two-dimensional domain $[0, L_x] \times [0, L_y]$, $k^2 = (n^2/L_x^2 + m^2/L_y^2)\pi^2$, where n and m are integers. λ is the eigenvalue which determines temporal growth. The steady state $\hat{S}$ is linearly stable if $\mathrm{Re}\lambda < 0$, for every eigenvalue λ of (6) (see, e.g., [11]).

Theorem 3.1. *The infection-free steady state $S_0 = (h/d_T, 0, 0)$ is linearly stable if $\mathcal{R}_0 < 1$, and unstable if $\mathcal{R}_0 > 1$*

Proof. For the infection-free steady state $S_0 = (h/d_T, 0, 0)$, we have

$$\mathrm{D}(S_0) = \begin{pmatrix} D_T & 0 & 0 \\ 0 & D_T & 0 \\ 0 & 0 & D_E \end{pmatrix}, \ \mathrm{A}(S_0) = \begin{pmatrix} -d_T & -\beta h/d_T & 0 \\ 0 & \beta h/d_T - d_I & 0 \\ 0 & 0 & -d_E \end{pmatrix},$$

and the characteristic equation of the linearized system at S_0 is

$$\begin{vmatrix} \lambda + D_T k^2 + d_T & \beta h/d_T & 0 \\ 0 & \lambda + D_T k^2 - \beta h/d_T + d_I & 0 \\ 0 & 0 & \lambda + D_E k^2 + d_E \end{vmatrix} = 0.$$

It has eigenvalues $\lambda_1 = -D_T k^2 - d_T$, $\lambda_2 = -D_T k^2 + \beta h/d_T - d_I$, $\lambda_3 = -D_E k^2 - d_E$. Note that $\lambda_1 < 0$, $\lambda_3 < 0$, and $\lambda_2 = -D_T k^2 + d_I(\mathcal{R}_0 - 1)$. If $\mathcal{R}_0 < 1$, then $\lambda_2 < 0$ for all k. Therefore, if $\mathcal{R}_0 < 1$, the steady state S_0 is linearly stable. If $\mathcal{R}_0 > 1$, then $\lambda_2 > 0$ for some small modes k, including $k = 0$, which means S_0 is unstable, completing the proof. □

Theorem 3.2. *The virus-persistence steady state $S_1 = (T_1, I_1, 0)$ is linearly stable if $\mathcal{R}_0 > 1$ and $cI_1 < d_E$ (i.e., $\mathcal{R}_0 > 1 + \beta d_E/cd_T$). It is unstable if $\mathcal{R}_0 < 1 + \beta d_E/cd_T$.*

Proof. For the steady state $S_1 = (T_1, I_1, 0)$, we have

$$\mathrm{D}(S_1) = \begin{pmatrix} D_T & 0 & 0 \\ 0 & D_T & 0 \\ 0 & 0 & D_E \end{pmatrix}, \ \mathrm{A}(S_1) = \begin{pmatrix} -d_T - \beta I_1 & -\beta T_1 & 0 \\ \beta I_1 & \beta T_1 - d_I & -pI_1 \\ 0 & 0 & cI_1 - d_E \end{pmatrix}.$$

Noticing that $\beta T_1 = d_I$ and $d_T + \beta I_1 = h\beta/d_I$, the characteristic polynomial of the linearized system at S_1 is given by

$$\begin{vmatrix} \lambda + D_T k^2 + h\beta/d_I & d_I & 0 \\ -h\beta/d_I + d_T & \lambda + D_T k^2 & pI_1 \\ 0 & 0 & \lambda + D_E k^2 - cI_1 + d_E \end{vmatrix} = 0.$$

One eigenvalue is $\lambda_1 = -D_E k^2 + cI_1 - d_E$, which is negative for all $k \geq 0$ as $cI_1 < d_E$. Other eigenvalues are determined by

$$\lambda^2 + a_1(k^2)\lambda + a_2(k^2) = 0, \tag{7}$$

where

$$\begin{aligned} a_1(k^2) &= 2D_T k^2 + \frac{h\beta}{d_I}, \\ a_2(k^2) &= D_T^2 k^4 + \frac{D_T h\beta}{d_I} k^2 + \frac{1}{d_I d_T}(\mathcal{R}_0 - 1). \end{aligned}$$

It is obvious that $a_1(k^2) > 0$ and $a_2(k^2) > 0$ if $\mathcal{R}_0 > 1$. Thus the roots of (7) have negative real parts for all k. Therefore, if $\mathcal{R}_0 > 1$ and $cI_1 < d_E$, the steady state S_1 is linearly stable. In contrarily, S_1 is unstable if $\mathcal{R}_0 < 1$ or $cI_1 > d_E$, since if $cI_1 > d_E$, $\lambda_1 > 0$ for some small k including $k = 0$; if $\mathcal{R}_0 < 1$, $a_2 < 0$ for some small k, which implies (7) has at least one eigenvalue with positive real part, completing the proof. □

Theorem 3.3. *Assume $cI_1 > d_E$ so that $S^* = (T^*, I^*, E^*)$ exists. Then it is linearly stable if $b_3(k^2) > 0$ and $b_1(k^2)b_2(k^2) - b_3(k^2) > 0$ for $k \geq 0$, where b_1, b_2 and b_3 are given below by (9), (10) and (11) respectively; otherwise, it is unstable.*

Proof. For the positive steady state S^*, the characteristic polynomial is given by

$$\begin{vmatrix} \lambda + D_T k^2 + d_T + \beta I^* & \beta T^* & 0 \\ -\beta I^* & \lambda + D_T k^2 & pI^* \\ 0 & \Psi^* k^2 - \frac{cE^*}{1+\eta E^*} & \lambda + D_E k^2 + d_E - \frac{cI^*}{(1+\eta E^*)^2} \end{vmatrix} = 0,$$

that is,

$$\lambda^3 + b_1(k^2)\lambda^2 + b_2(k^2)\lambda + b_3(k^2) = 0. \tag{8}$$

Here

$$b_1(k^2) = (2D_T + D_E)k^2 + d_T + \beta I^* + d_E\left(1 - \frac{1}{1+\eta E^*}\right) > 0, \tag{9}$$

$$b_2(k^2) = c_1 k^4 + c_2 k^2 + c_3, \tag{10}$$

where

$$\begin{aligned} c_1 &= D_T^2 + 2D_T D_E > 0, \\ c_2 &= (D_T + D_E)(d_T + \beta I^*) + 2D_T d_E\left(1 - \frac{1}{1+\eta E^*}\right) - pI^*\Psi^*, \\ c_3 &= (d_T + \beta I^*)d_E\left(1 - \frac{1}{1+\eta E^*}\right) + pd_E E^* + \beta^2 I^* T^* > 0, \end{aligned}$$

$$b_3(k^2) = d_1 k^6 + d_2 k^4 + d_3 k^2 + d_4, \tag{11}$$

where

$$\begin{aligned}
d_1 &= D_T^2 D_E > 0,\\
d_2 &= D_T\left[D_E(d_T+\beta I^*)+D_T d_E\left(1-\frac{1}{1+\eta E^*}\right)\right]-D_T p I^*\Psi^*,\\
d_3 &= D_T(d_T+\beta I^*)d_E\left(1-\frac{1}{1+\eta E^*}\right)+D_T p d_E E^*+D_E\beta^2 T^* I^*\\
&\quad -(d_T+\beta I^*)pI^*\Psi^*,\\
d_4 &= pd_E E^*(d_T+\beta I^*)+\beta^2 T^* I^* d_E\left(1-\frac{1}{1+\eta E^*}\right)>0,
\end{aligned}$$

Also

$$b_1(k^2)b_2(k^2)-b_3(k^2)=h_1k^6+h_2k^4+h_3k^2+h_4, \tag{12}$$

where

$$\begin{aligned}
h_1 &= 2D_T(D_T+D_E)^2>0,\\
h_2 &= (D_T+D_E)\left[(d_T+\beta I^*)(3D_T+D_E)+4D_T d_E\left(1-\frac{1}{1+\eta E^*}\right)\right]\\
&\quad -(D_T+D_E)pI^*\Psi^*,\\
h_3 &= 2D_T\beta^2 I^*T^*+(D_T+D_E)\left[pd_E E^*+(d_T+\beta I^*)^2\right]\\
&\quad +2\left[(2D_T+D_E)(d_T+\beta I^*)+D_T d_E\left(1-\frac{1}{1+\eta E^*}\right)\right]d_E\left(1-\frac{1}{1+\eta E^*}\right)\\
&\quad -d_E\left(1-\frac{1}{1+\eta E^*}\right)pI^*\Psi^*,\\
h_4 &= \left[(d_T+\beta I^*)^2+(d_T+\beta I^*)d_E\left(1-\frac{1}{1+\eta E^*}\right)+pd_E E^*\right]\\
&\quad \times d_E\left(1-\frac{1}{1+\eta E^*}\right)+(d_T+\beta I^*)\beta^2 I^*T^*>0.
\end{aligned}$$

By Routh-Hurwitz Criteria, $Re(\lambda)<0$ for every eigenvalue λ if and only if $b_1(k^2)>0$, $b_3(k^2)>0$ and $b_1(k^2)b_2(k^2)-b_3(k^2)$ for $k\geq 0$. Note that $b_1(k^2)>0$ for $k\geq 0$. Therefore, S^* is linearly stable if and only if $b_3(k^2)>0$ and $b_1(k^2)b_2(k^2)-b_3(k^2)$ for $k\geq 0$. □

Notice that, in the absence of diffusion, that is, in the spatial homogeneous case ($k=0$), $b_3(0)=d_4>0$ and $b_1(0)b_2(0)-b_3(0)=h_4>0$, which imply that the positive steady state S^* is linearly stable if it exists, that is, if $cI_1>d_E$. In contrast, under the same condition, the homogeneous steady state S^* can be unstable to small spatial perturbations when diffusion is present, for instance if $b_3(k^2)<0$ or $b_1(k^2)b_2(k^2)-b_3(k^2)<0$ for some modes k. This diffusion-driven instability is called Turing instability [11].

4. **Turing instability and pattern formation.** Among the two conditions $b_3(k^2)>0$ and $b_1(k^2)b_2(k^2)-b_3(k^2)$ for $k\geq 0$ in Theorem 3.3 that ensure the stability of S^*, violation of each will lead to different consequences: when $b_3(k^2)$ changes from positive to negative, typically there will be steady state bifurcation resulting in occurrence of a spatially heterogeneous steady state; whereas when $b_1(k^2)b_2(k^2)-b_3(k^2)$ changes from positive to negative, Hopf bifurcation will occur causing temporally periodic solution oscillating about the constant steady state S^*

(see, e.g., Yu [19]). Thus, it is worthwhile to explore the possible sign changes for those two quantities.

We expect spatial pattern formation when the homogeneous positive steady state S^* loses its stability, that is when $b_3(k^2) < 0$ or $b_1(k^2)b_2(k^2) - b_3(k^2) < 0$. To investigate conditions for Turing instability, we denote $\phi_d(s) =: b_3(s)$ and $\phi_h(s) =: b_1(s)b_2(s) - b_3(s)$, that is

$$\phi_d(s) = d_1 s^3 + d_2 s^2 + d_3 s + d_4, \quad \phi_h(s) = h_1 s^3 + h_2 s^2 + h_3 s + h_4,$$

where s is assumed to be $s \in \mathbb{R}$. We see that $\phi_d(s)$ has a negative root, since $d_1 > 0$, $\phi_d(-\infty) = -\infty$ and $\phi_d(0) = d_4 > 0$. Now if $d_2 \geq 0$ and $d_3 \geq 0$, then $\phi_d(s) > 0$ for $s \geq 0$, and there is no bifurcation. We only need to worry the case of either $d_2 < 0$ or $d_3 < 0$ for which $\phi_d(s)$ may have two (up to multiplicity) or no positive roots, by the Descarte's rule of signs, and in the latter case, $b_3(k^2) = \phi_d(s)$ remains positive for all $s \geq 0$. A steady state bifurcation occurs if $\phi_d(s)$ has two distinct positive roots. The conditions for the existence of two distinct positive roots of $\phi_d(s)$ can be determined by the sign of $\phi_d(s_+^d)$, where s_+^d is one of the roots of $\phi_d'(s) = 3d_1 s^2 + 2d_2 s + d_3$, say

$$s_\pm^d = \frac{1}{3d_1}\left(-d_2 \pm \sqrt{d_2^2 - 3d_1 d_3}\right).$$

According the the signs of d_2 and d_3, we have the following three cases.

(i) If $d_3 < 0$, then $\sqrt{d_2^2 - 3d_1 d_3} > |d_2|$, $s_+^d > 0$ and $s_-^d < 0$. In this case, $\phi_d(s)$ has two distinct positive roots, if and only if $\phi_d(s_+^d) < 0$.

(ii) If $d_3 > 0$ and $d_2 < 0$, then for different cases of $d_2^2 - 3d_1 d_3$, we have that
(ii)-1 $d_2^2 - 3d_1 d_3 > 0 \Longrightarrow \sqrt{d_2^2 - 3d_1 d_3} < |d_2| \Longrightarrow s_+^d > s_-^d > 0$;
(ii)-2 $d_2^2 - 3d_1 d_3 = 0 \Longrightarrow s_\pm^d = -\frac{d_2}{3d_1} > 0 \Longrightarrow \phi_d'(s) \geq 0$ for $s \in \mathbb{R}$;
(ii)-3 $d_2^2 - 3d_1 d_3 < 0 \Longrightarrow \phi_d'(s) > 0$ for $s \in \mathbb{R}$.
In the case (ii)-1, $\phi_d(s)$ has two positive roots, if and only if $\phi_d(s_+^d) < 0$, and in the cases (ii)-2 and (ii)-3, $\phi_d(s)$ does not have any positive root and $\phi_d(s) > 0$ for $s \geq 0$.

(iii) If $d_3 = 0$ and $d_2 < 0$, then $s_+^d > 0$, $s_-^d = 0$, and $\phi_d(s)$ has two distinct positive roots if and only if $\phi_d(s_+^d) < 0$.

From the above, we conclude that $\phi_d(s)$ has two positive roots if one of the following conditions is satisfied.
(C1) $d_3 < 0$, $\phi_d(s_+^d) < 0$;
(C2) $d_3 \geq 0$, $d_2 < 0$, $d_2^2 - 3d_1 d_3 > 0$, $\phi_d(s_+^d) < 0$;
In these cases, for some values of $s = k^2$, $b_3(k^2)$ becomes negative destroying the stability of S^*.

Similarly, let $\phi_h(s) =: b_1(s)b_2(s) - b_3^2(s) = h_1 s^3 + h_2 s^2 + h_3 s + h_4$ and denote

$$s_\pm^h = \frac{1}{3h_1}\left(-h_2 \pm \sqrt{h_2^2 - 3h_1 h_3}\right).$$

Then, $\phi_h(s)$ can become negative only when it has two positive real roots, and this is implied by one of the following two conditions:
(C3) $h_3 < 0$, $\phi_h(s_+^h) < 0$;
(C4) $h_3 \geq 0$, $h_2 < 0$, $h_2^2 - 3h_1 h_3 > 0$, $\phi_h(s_+^h) < 0$.

Turing instability may occur if one of the conditions (C1)-(C4) is satisfied, resulting formation of patterns. Notice that the formula of $\phi_d(s_+^d)$ can be simplified

to the following form

$$\phi_d(s_+^d) = \frac{2}{3}\left(d_3 - \frac{d_2^2}{3d_1}\right)s_+^d + \left(d_4 - \frac{d_2 d_3}{9d_1}\right),$$

applying the fact that $\phi_d'(s_+^d) = 3d_1(s_+^d)^2 + 2d_2 s_+^d + d_3 = 0$.

A challenging problem for chemotaxis models is the blow-up of solutions in finite time. Blow-up of solutions implies the whole population concentrate in a single point in a finite time. To avoid a blow-up, various mechanisms are introduced [7, 8, 14, 17]. One mechanism is to consider the volume-filling effect [12, 17], which supposes only a finite number of cells can be accommodated at any site. We assume the chemotactic response function has the form $\Psi(E, I) = \chi(I)q(E)$, where the chemotactic sensitivity function $\chi(I)$ is chosen to be a constant χ. The volume-filling effect is described by $q(E)$ satisfying $q(E_M) = 0$, and $q(E) \geq 0$ for all $0 \leq E < E_M$, where E_M is the upper bound of the CTLs population E in the model, which shows the maximum number of cells those can be accommodated at any site. The function $q(E)$ is considered as the probability of the cells finding a space at its neighboring location depends upon the availability of space. In this paper, we choose a simple form $q(E) = 1 - \frac{E}{E_M}$ for the volume-filling effect of CTLs to prevent the blow-up of solutions of the model. Thus we adopt the following form for the chemosensitivity function $\Psi(E, I)$:

$$\Psi(E, I) = \chi\left(1 - \frac{E}{E_M}\right), \quad \text{for a chemorepulsion system} \tag{13}$$

and

$$\Psi(E, I) = -\chi\left(1 - \frac{E}{E_M}\right), \quad \text{for a chemoattraction system.} \tag{14}$$

Furthermore, we have

$$\Psi^* = \chi E^*\left(1 - \frac{E^*}{E_M}\right) > 0, \quad \text{for a chemorepulsion system} \tag{15}$$

and

$$\Psi^* = -\chi E^*\left(1 - \frac{E^*}{E_M}\right) < 0, \quad \text{for a chemoattraction system.} \tag{16}$$

For a chemoattraction system, $\Psi^* < 0$ implies that d_2, d_4, h_2 and h_4 are all positive, meaning that S^* is always linearly stable and thus, Turing instability will not occur. However, for a chemorepulsion system, Turing instability may occur. To demonstrate this we choose χ, the strength of the chemotactic sensitivity, as the bifurcation parameter and numerically explore the occurrence of Turing instability. Naturally, one would expect that there exists a critical value χ_c such that there is no pattern formation if $\chi < \chi_c$, while pattern will be formed if $\chi > \chi_c$. Notice that d_1, d_4, h_1 and h_4 are independent of χ, while $d_2(\chi)$, $d_3(\chi)$, $h_2(\chi)$ and $h_3(\chi)$ are linear strictly decreasing functions of χ, with $d_j(0) > 0$, $h_j(0) > 0$, $d_j(+\infty) = -\infty$, and $h_j(+\infty) = -\infty$, $(j = 2, 3)$. Thus, $d_2^2(\chi) - 3d_1 d_3(\chi)$ and $h_2^2(\chi) - 3h_1 h_3(\chi)$ are quadratic functions, which tend to positive infinity as $\chi \to +\infty$. Furthermore, $[\phi_d(s_+^d)](\chi) \to -\infty$, $[\phi_h(s_+^h)](\chi) \to -\infty$, as $\chi \to +\infty$. Therefore, as χ increases, at least one of the conditions (C1)-(C4) holds. The Turing instability threshold values can be determined according to the conditions (C1)-(C4).

For example, to determine the threshold for steady state bifurcation, let χ_2^d and χ_3^d be the roots of $d_2(\chi) = 0$ and $d_3(\chi) = 0$ respectively, that is, $d_2(\chi_2^d) = 0$

and $d_3(\chi_3^d) = 0$. If $\chi_3^d \leq \chi_2^d$, then at $\chi = \chi_3^d$, we have $d_3 = 0$, $d_2 \geq 0$, $s_+^d = 0$ and $\phi_d(s_+^d) = d_4 > 0$. Let χ_1^S be the smallest value that satisfies $\chi_1^S > \chi_3^d$, $[\phi_d(s_+^d)](\chi_1^S) = 0$, and $[\phi_d(s_+^d)](\chi) < 0$ for $\chi_1^S < \chi < \chi_1^S + \delta_1$, where $\delta_1 > 0$. Then the condition (C1) holds for $\chi_1^S < \chi < \chi_1^S + \delta_1$.

In contrast, if $\chi_2^d < \chi_3^d$, then at $\chi = \chi_2^d$, we have $d_2 = 0$, $d_3 > 0$, $d_2^2 - 3d_1d_3 = -3d_1d_3 < 0$. Let χ_4^d be the root of $d_2^2(\chi) - 3d_1(\chi)d_3(\chi) = 0$ satisfying $\chi_4 > \chi_2$, then $\chi_4^d < \chi_3^d$. At χ_4^d, we have $d_2^2 - 3d_1d_3 = 0$, $d_3 > 0$, $d_2 < 0$, and $[\phi_d(s_+^d)](\chi_4^d) = d_4 - \frac{d_2 d_3}{9d_1} > 0$. The condition (C2) does not hold for $\chi \leq \chi_4^d$. Let χ_2^S be the smallest value that satisfies $\chi_2^S > \chi_4^d$, $[\phi_d(s_+^d)](\chi_2^S) = 0$, and $[\phi_d(s_+^d)](\chi) < 0$ for $\chi_2^S < \chi < \chi_2^S + \delta_2$, where $\delta_2 > 0$. In this case, if $\chi_2^S \leq \chi_3^d$, then the condition (C2) holds for $\chi_2^S < \chi < \chi_2^S + \delta_2$, while the condition (C1) holds for $\chi_2^S < \chi < \chi_2^S + \delta_2$ if $\chi_2^S > \chi_3^d$.

Therefore, the value χ_1^S or χ_2^S, which is determined by the roots of $[\phi_d(s_+^d)](\chi) = 0$, presents the threshold for steady state bifurcation. Similarly, the threshold value χ_1^H or χ_2^H for Hopf bifurcation can be derived according to the conditions (C3) and (C4), which is determined by the roots of $[\phi_h(s_+^h)](\chi) = 0$.

From the above analysis, we know that S^* may lose its stability leading to bifurcation when $\phi_d(s_+^d) = 0$ or $\phi_h(s_+^h) = 0$. The bifurcation occurs at critical values $\chi = \chi_c^S$ and $\chi = \chi_c^H$ which are determined by $\phi_d(s_+^d)\big|_{\chi_c^S} = 0$ and $\phi_h(s_+^h)\big|_{\chi_c^H} = 0$. Among these two critical values, χ_c^S is a steady state bifurcation value, while χ_c^H is a Hopf bifurcation value. If $\chi_c^S < \chi_c^H$ and $\chi_c^S < \chi$, $\phi_d(s)$ has two positive solutions s_1^d and s_2^d which give a range of unstable wave numbers $k^2 \in (s_1^d, s_2^d)$. Similarly, if $\chi_c^H < \chi_c^S$ and $\chi_c^H < \chi$, $\phi_h(s)$ has two positive solutions s_1^h and s_2^h which also give a range of unstable wave numbers $k^2 \in (s_1^h, s_2^h)$.

Notice that when we derive the bifurcation thresholds, we assumed s (i.e k^2) to be continuum. However, with finite spatial domains, there is a discrete set of possible modes k as mentioned above. Therefore, the threshold values χ_c^S and χ_c^H obtained here may be not the exact bifurcation values. χ_c^S and χ_c^H give the lower bound of the bifurcation values. The exact bifurcation values may be somewhat greater than χ_c^S and χ_c^H, depending on the size of the domain and the shapes of $\phi_d(s)$ and $\phi_h(s)$.

In a special case, if the uninfected cells and infected cells cannot diffuse ($D_T = 0$), we have $d_1 = 0$, $d_2 = 0$ and $h_1 = 0$. Thus $\phi_d(s) = d_3 s + d_4$ and $\phi_h(s) = h_2 s^2 + h_3 s + h_4$. It is easy to see that the Turing instability conditions change to (H1) $d_3 < 0$, or (H2) $h_2 < 0$, or (H3) $h_2 \geq 0$, $h_3 < 0$, $h_3^2 - 4h_2h_4 > 0$. If (H1) holds, a steady state bifurcation occurs, while there is a Hopf bifurcation if any of (H2) and (H3) is satisfied. The threshold value for steady bifurcation is $\chi_c^S = \chi_3^d$, the root of $d_3(\chi) = 0$. From the formulas of h_2 and h_3, we know that the root χ_2^h of $h_2(\chi) = 0$ is always smaller than the root χ_3^h of $h_3(\chi) = 0$. Thus, the threshold value for Hopf bifurcation is $\chi_c^H = \chi_2^h$, according to the conditions (H2) and (H3).

5. **Numerical simulation.**

In this section, we use the framework of section 4 to perform some numerical simulations to explore the aforementioned bifurcations. To this end, we choose χ as the bifurcation parameter and other baseline parameters as $h = 10$, $d_T = 0.1$, $d_I = 0.2$, $d_E = 0.1$, $\beta = 0.1$, $p = 0.5$, $c = 0.2$, $\eta = 0.01$ and $E_M = 2000$, then $\mathcal{R}_0 = 50 > 1$, $I_1 - \frac{d_E}{c} = 48.5 > 0$, and $S^* = (64.0197, 0.5620, 12.4039)$. The space is assumed to be one-dimensional and $\Omega = [0, l\pi]$, then $k^2 = n^2/l^2$, where n is an integer and $l = 3$. In what follows, we suppose that k assumes

continuous values (i.e. s is continuous), in order to derive the threshold values of χ for bifurcation. We choose $\Psi(E, I)$ as (13), and χ as the bifurcation parameter.

First, we consider the case $D_T = 0$. Assuming $D_E = 1$, we obtain $\chi_c^S = \chi_3^d = 0.6650$ and $\chi_c^H = \chi_2^h = 0.0451$ (see Fig. 2-(a) and (b)). Since $\chi_c^H < \chi_c^S$, Hopf bifurcation may occur at $\chi = \chi_c^H = 0.0451$, and pattern forms for $\chi > \chi_c^H$. Fig. 1 shows the pattern formation of the model when $\chi = 0.5$ and $\chi = 0.6$. We can determine the unstable wave modes from Fig. 2-(c). For $\chi = 0.05$, the zero point of $\phi_h(s) = 0$ is $s_1 = 38.1088$, and $\phi_h(s) < 0$ for $s > s_1$. The minimal unstable mode $k_1 = n_1/l$ is the smallest $k = n/l$ that greater than $\sqrt{s_1} = 6.1732$. Here, we obtain $n_1 = 19$, and pattern forms for modes $k = n/l$, where $n \geq 19$. Similarly, for $\chi = 0.06$, we obtain that the zero point of $\phi_h(s) = 0$ is $s_2 = 12.6025$, and the unstable wave modes are $k = n/l$, where $n \geq 11$.

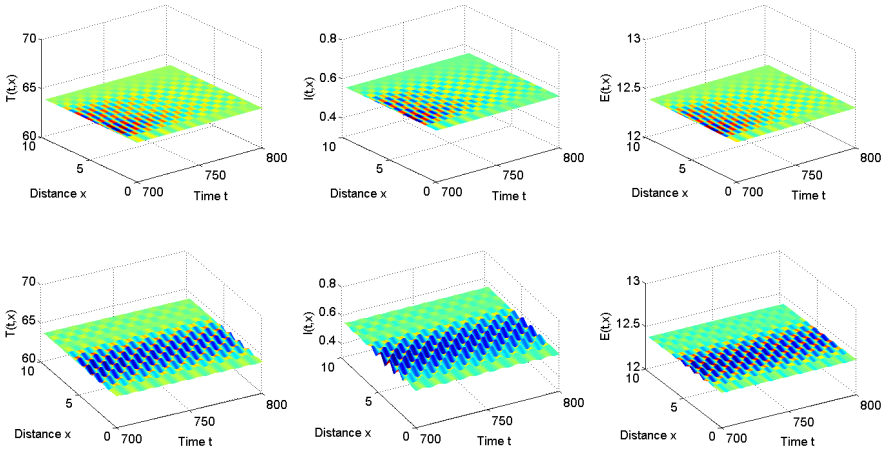

FIGURE 1. Temporal and spatial evolution of $T(x,t)$, $I(x,t)$ and $E(x,t)$. First row: $\chi = 0.05$. Second row: $\chi = 0.06$.

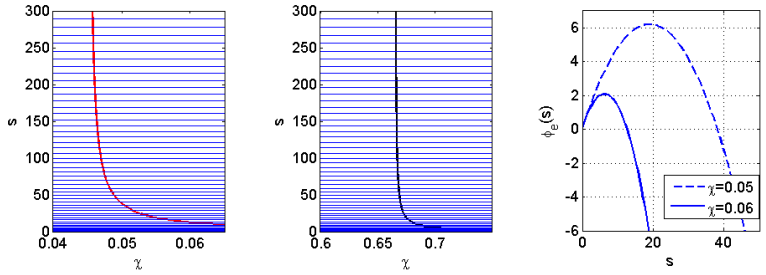

(a) (b) (c)

FIGURE 2. (a) Graph of $\phi_h(s, \chi) = h_2(\chi)s^2 + h_3(\chi)s + h_4 = 0$. (b) Graph of $\phi_d(s, \chi) = d_3(\chi)s + d_4 = 0$. The horizontal lines are $s = n^2/l^2$, where $l = 3$, and n is a positive integer, $1 \leq n \leq 51$. (c) Graphs of $\phi_e(s)$ when $\chi = 0.05$ and $\chi = 0.06$.

Next we consider the case when $D_T > 0$. To show two different bifurcations, steady state bifurcation and Hopf bifurcation, we choose two sets of different diffusion rates of the populations: (I) $D_T = 0.005$, $D_E = 0.1$, and (II) $D_T = 0.1$, $D_E = 0.1$. For the case (I), we see from Fig. 3-(a) that steady state bifurcation may occur for some modes k and some range of χ, and Hopf bifurcation can also occur for some other modes k and χ. In contrast, for the case (II), Fig. 3-(b) shows that steady state bifurcation may occur for some wave modes k, and Hopf bifurcation cannot occur, since χ satisfying $b_3 = 0$ (i.e. $\phi_d = 0$) is always smaller than χ satisfying $b_1 b_2 - b_3 = 0$ (i.e. $\phi_h = 0$), for all modes k.

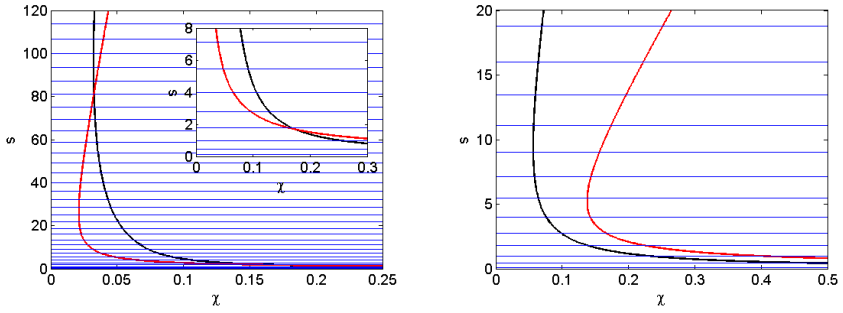

FIGURE 3. Graphs of $\phi_d(s,\chi) = d_1 s^3 + d_2(\chi)s^2 + d_3(\chi)s + d_4 = 0$ (black) and $\phi_h(s,\chi) = h_1 s^3 + h_2(\chi)s^2 + h_3(\chi)s + h_4 = 0$ (red). (a) $D_T = 0.005$, $D_E = 0.1$. (b) $D_T = 0.1$, $D_E = 0.1$. The horizontal lines are $s = n^2/l^2$, where $l = 3$, and n is a positive integer, (a) $1 \le n \le 35$, (b) $1 \le n \le 13$.

For the case (I), that is, when $D_T = 0.005$ and $D_E = 0.1$, the curves of $d_2^2(\chi) - 3d_1 d_3(\chi)$, $[\phi_d(s_+^d)](\chi)$, $h_2^2(\chi) - 3h_1 h_3(\chi)$ and $[\phi_h(s_+^h)](\chi)$ are shown in Fig. 4-(a), Fig. 4-(b), Fig. 4-(c) and Fig. 4-(d) respectively. The roots of these functions in the corresponding regions are $\chi_0^d = 0.0288$, $\chi_c^d = 0.0321$, $\chi_0^h = 0.0186$ and $\chi_c^h = 0.0209$ respectively. The functions $d_2(\chi)$, $d_3(\chi)$, $h_2(\chi)$ and $h_3(\chi)$ are linear strictly decreasing functions of χ, and roots of these functions are given by $\chi_2^d = 0.0045$, $\chi_3^d = 0.0722$, $\chi_2^h = 0.0052$ and $\chi_3^h = 1.8747$ respectively.

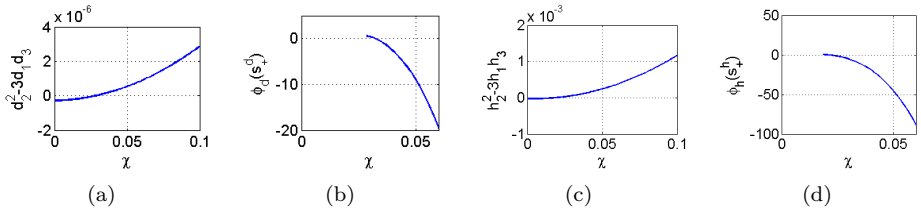

FIGURE 4. (a) $d_2^2(\chi) - 3d_1 d_3(\chi)$. One zero point: $\chi = 0.0288$. (b) $[\phi_d(s_+^d)](\chi)$. One zero point: $\chi = 0.0321$. (c) $h_2^2(\chi) - 3h_1 h_3(\chi)$. One zero point: $\chi = 0.0186$. (d) $[\phi_h(s_+^h)](\chi)$. One zero point: $\chi = 0.0209$.

Applying the bifurcation conditions (C1)-(C4), we find the bifurcation threshold values $\chi_c^S = \chi_c^d = 0.0321$ and $\chi_c^H = \chi_c^h = 0.0209$. Since $\chi_c^H < \chi_c^S$, Hopf bifurcation may occur at $\chi = \chi_c^H$ and temporal periodic and spatial inhomogeneous pattern forms for $\chi_H^H < \chi < \chi_c^S$. For $\chi > \chi_c^S$, the positive steady state is unstable and spatial heterogeneous pattern forms, which may be not temporal periodic.

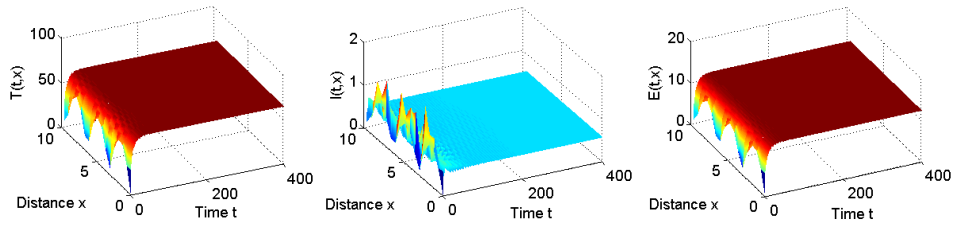

FIGURE 5. Temporal and spatial evolution of $T(x,t)$, $I(x,t)$ and $E(x,t)$. The homogenous positive steady state S^* is stable when $\chi = 0.02\ (< \chi_c^H)$.

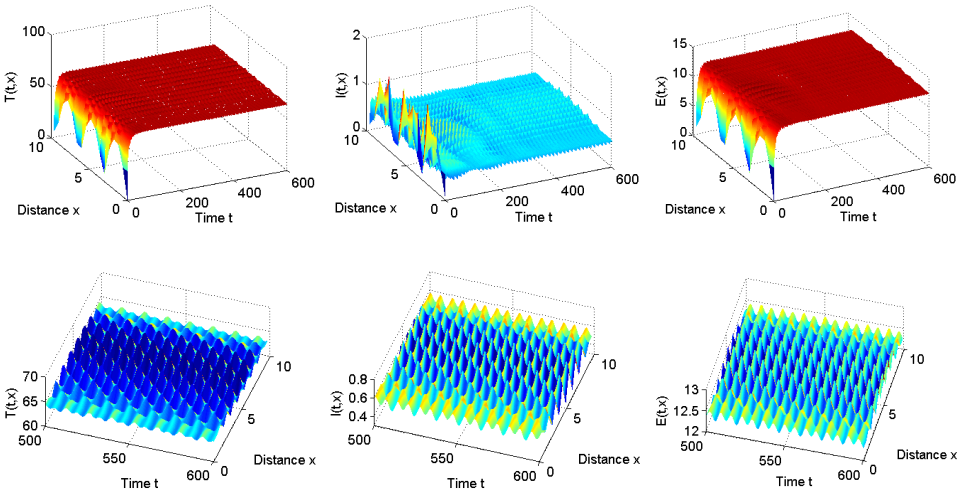

FIGURE 6. Temporal and spatial evolution of $T(x,t)$, $I(x,t)$ and $E(x,t)$. when $\chi = 0.029$ ($\chi_c^H < \chi = 0.029 < \chi_c^S$). The homogeneous positive steady state S^* is unstable, and spatial patterns are formed.

Fig. 5 shows that the positive steady state S^* is stable as $\chi = 0.02 < \chi_c^H$. As χ increases so that $\chi > \chi_c^H$ but $\chi < \chi_c^S$, the positive steady state S^* becomes unstable, and Hopf bifurcation occurs. Fig. 6 shows the temporal and spatial evolution of $T(x,t)$, $I(x,t)$ and $E(x,t)$. From the end part of the these time evolution figures (i.e., the figures in second row of Fig. 6), we see the form of spatial patterns and temporal periodicity of the solutions. Fig. 7 shows the periodic solutions at space locations $x = 1.5\pi$ and $x = 3\pi$. The amplitudes of the periodic solutions vary in

different space locations as shown in Fig. 7. We see that the amplitudes at $x = 1.5\pi$ are greater than those at $x = 3\pi$ for $T(x,t)$, $I(x,t)$ and $E(x,t)$ respectively. When $\chi = 0.033$ which exceeds the threshold value χ_c^S, the positive steady state also loses its stability and spatial heterogeneous pattern forms, which may be not periodic, as shown in Fig. 8.

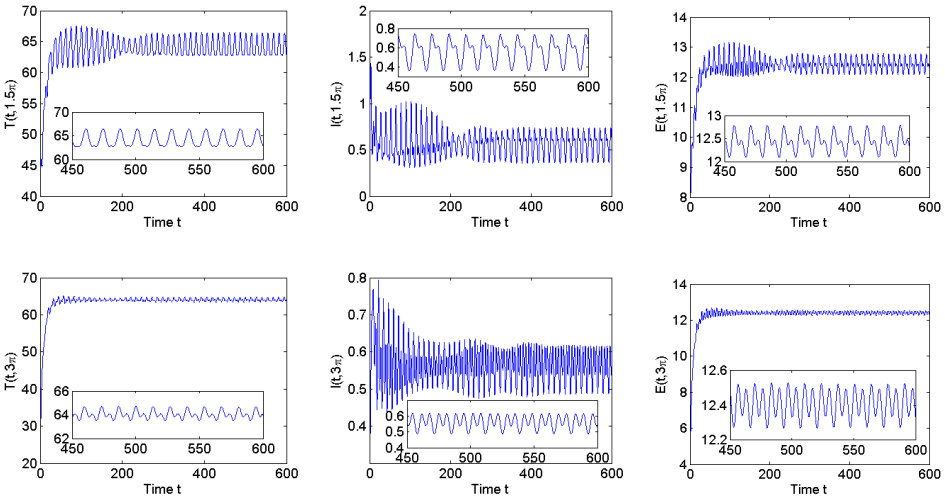

FIGURE 7. Temporal evolution of $T(x,t)$, $I(x,t)$ and $E(x,t)$. First row: $x = 1.5\pi$; Second row: $x = 3\pi$. When $\chi = 0.029$ ($\chi_c^H < \chi = 0.029 < \chi_c^S$), Hopf bifurcation occurs for the system, and there are periodic solutions.

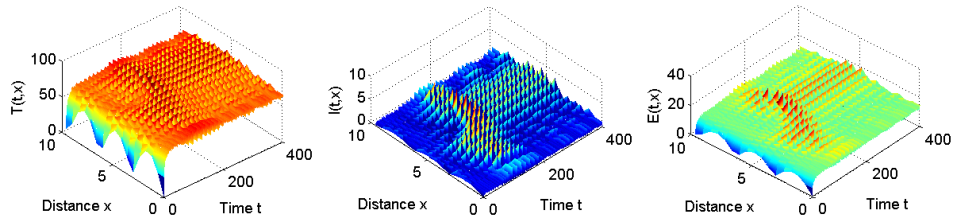

FIGURE 8. Temporal and spatial evolution of $T(x,t)$, $I(x,t)$ and $E(x,t)$. The homogenous positive steady state S^* is unstable and spatial patterns form when $\chi = 0.033$ ($> \chi_c^S$).

For the case (II), that is, when $D_T = 0.1$ and $D_E = 0.1$, Fig. 9-(a) and Fig. 9-(b) show the curves of $d_2^2(\chi) - 3d_1d_3(\chi)$ and $[\phi_d(s_+^d)](\chi)$ respectively, as Fig. 9-(c) and Fig. 9-(d) show the curves of $h_2^2(\chi) - 3h_1h_3(\chi)$ and $[\phi_h(s_+^h)](\chi)$ respectively. Roots of these functions in the corresponding regions are $\chi_0^d = 0.0474$, $\chi_c^d = 0.0561$, $\chi_0^h = 0.1187$ and $\chi_c^h = 0.1373$ respectively. The functions $d_2(\chi)$, $d_3(\chi)$, $h_2(\chi)$ and $h_3(\chi)$ are linear strictly decreasing functions of χ, and roots of these functions are given by $\chi_2^d = 0.0048$, $\chi_3^d = 0.1814$, $\chi_2^h = 0.0193$ and $\chi_3^h = 5.2828$ respectively.

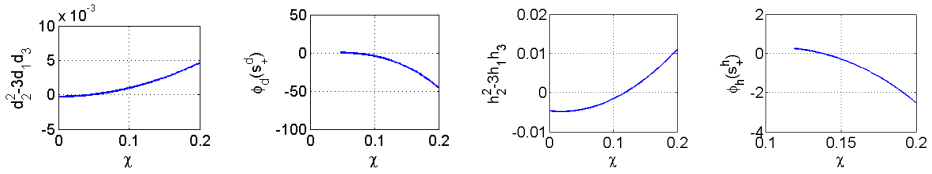

FIGURE 9. (a) $d_2(\chi)^2-3d_1d_3(\chi)$. One zero point: $\chi = 0.0474$. (b) $[\phi_d(s_+^d)](\chi)$. One zero point: $\chi = 0.0561$. (c) $h_2(\chi)^2 - 3h_1h_3(\chi)$. One zero point: $\chi = 0.1187$. (d) $[\phi_h(s_+^h)](\chi)$. One zero point: $\chi = 0.01373$.

Applying the bifurcation conditions (C1)-(C4), we obtain the bifurcation values $\chi_c^S = \chi_c^d = 0.0561$ and $\chi_c^H = \chi_c^h = 0.1373$. Since $\chi_c^S < \chi_c^H$, we know that steady state bifurcation may occur at $\chi = \chi_c^S$ and spatial pattern forms for $\chi > \chi_c^S$. The positive steady state S^* is stable when χ is less than the steady state bifurcation value χ_c^S. However, when χ exceeds the bifurcation value χ_c^S, the positive steady state loses its stability and spatial inhomogeneous pattern forms, as shown in Fig. 10, where $\chi = 0.06$. In this case, Hopf bifurcation cannot occur, which can be seen from Fig. 3-(b), showing that $b_3(\chi)$ always reaches zero before $b_1(\chi)b_2(\chi) - b_3(\chi)$ reaching zero for all mode $k \geq 0$.

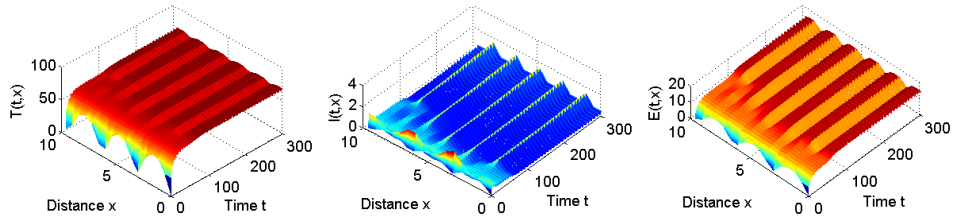

FIGURE 10. Temporal and spatial evolution of $T(x,t)$, $I(x,t)$ and $E(x,t)$. The homogenous positive steady state is unstable and spatial patterns form when $\chi = 0.06$ ($> \chi_c^S$).

6. **Conclusion and discussion.** In this paper, we have studied the effect of chemotactic movement, including chemoattaction and chemorepulsion, of CTLs on the HIV-1 infection dynamics by a reaction diffusion model with chemotaxis. In the absence of spatial effect, that is, without random diffusion and chemotactic movement, the homogeneous positive steady state is locally stable. Choosing the typical chemotactic sensitivity function (14), we found that chemoattraction movement of CTLs also cannot destabilize the homogeneous positive steady state, and there is no heterogeneous pattern formation.

In contrast, chemorepulsion movement of CTLs can lead to instability of the homogeneous positive steady state and formation of spatially heterogeneous patterns. Using the typical chemotactic sensitivity function (13) and choosing the strength of chemotactic sensitivity χ as the bifurcation parameter, we found that Turing

instability occurs when χ exceeds some threshold. The bifurcation may be steady state bifurcation or Hopf bifurcation depending on χ and other parameters, such as the diffusion coefficients D_T and D_E. We identified four conditions (C1)-(C4) from which bifurcation thresholds may be derived. With a finite domain in one dimensional space, we demonstrated the stability of positive steady state, steady state bifurcation and Hopf bifurcation for different diffusion coefficients D_T and D_E and chemotactic sensitivities χ.

The chemotactic movement of CTLs leads to the instability of the homogeneous positive steady state and pattern formation or periodic solutions of the system for some range of parameter values. With stable patterns or periodic solutions, the concentration of infected cells and virus load cannot stabilize at a constant level, but show heterogeneous distributions or oscillations. This is important for experimental or clinic estimation of virus load. Due to the heterogeneous distributions or periodic oscillations, lower (or higher) virus load detected at a site and at a moment does not indicate the same lower (or higher) load at different sites for a long time. The oscillations of viral load levels in the plasma are also plausible under the effects of immune responses or delays in the virus infection dynamics (e.g., see [6]).

In order for CTLs to successfully control HIV-1 infection, they must home efficiently to infected tissue sites and migrate within the infected tissue to the virus-infected cells. In this paper, we only considered the chemotactic sensitivity functions (13) and (14) for chemorepulsion and chemoattraction models respectively. For the chemoattraction model with (14), the negativity of Ψ^* drives the positive steady state to be stable. If other chemotactic sensitivity functions are chosen so that Ψ^* is not always negative, then it is possible that Turing bifurcations may also occur for chemoattraction model. For example, for the Macroscopic form of Lapidus and Schiller (with receptor response law)[10],

$$\chi(I) = -\frac{\rho}{(K+I)^2},$$

we have

$$\Psi^* = -E^* \left(1 - \frac{E^*}{E_M}\right) \frac{\rho}{(K+I^*)^2} \left(1 - \frac{2}{K+I^*}\right),$$

which is positive for some K. For small K, there may be Turing bifurcation and pattern formation. More intensive investigation is needed for this, which is left as possible future work.

In our chemorepulsion model, the chemotactic sensitivity is assumed to be constant and positive. However, some experiments (e.g., [4]) demonstrate that gp120 elicits bidirectional T-cell movement in a receptor-mediated, concentration-dependent manner, attracting $CD8^+$ lymphocytes and HIV-specific CTLs maximally at low concentration of gp120 and repelling the same cells at a higher concentration of gp120. Therefore, the chemotactic sensitivity function should be negative (chemoattraction) for low concentration of gp120 and positive (chemorepulsion) for high concentration of gp120. Relating to our simplified model, the chemotactic sensitivity function should be negative (chemoattraction) for low level of $I(x,t)$ and positive for high level of $I(x,t)$. Considering this in our model, the analysis would be more difficult mathematically, and is thus also left for our future work.

REFERENCES

[1] R. A. Adams, *Sobolev Spaces*, Academic Press, New York, 1975.

[2] H. Amann, Dynamcial theory of quasilinear parabolic equations III: Global existence, *Math. Z.*, **202** (1989), 219–250.
[3] H. Amann, Nonhomogeneous linear and quasilinear elliptic and parabolic boundary value problems, in: *Schmeisser H.J., Triebel H. (Eds.),Function spaces, Differential Operators and Nonlinear Analysis*, *Teubner Texte Math.*, **133** (1993), 9–126.
[4] D. M. Brainard et al, Migration of antigen-specific T cells away from CXCR4-binding Human Immunodeficiency Virus Type 1 gp120, *J. Virol.*, **78** (2004), 5184–5193.
[5] D. M. Brainard et al, Decreased CXCR3$^+$ CD8 T cells in Advanced Human Immunodeficiency Virus infection suggest that a homing defect contributes to cytotoxic T-lymphocyte dysfunction, *J. Virol.*, **81** (2007), 8439–8450.
[6] M. S. Ciupe, B. L. Bivort, D. M. Bortz and P. W. Nelson, Estimating kinetic parameters from HIV primary infection data through the eyes of three different mathematical models, *Math. Biosci.*, **200** (2006), 1–27.
[7] T. Hillen and K. Painter, Global existence for a parabolic chemotaxis model with prevention of overcrowding, *Advances in Appl. Math.*, **26** (2001), 280–301.
[8] T. Hillen and K. J. Painter, A user's guide to PDE models for chemotaxis, *J. Math. Biol.*, **58** (2009), 183–217.
[9] Y. Lou and X. Q. Zhao, A reaction-diffusion malaria model with incubation period in the vector population, *J. Math. Biol.*, **62** (2011), 543–568.
[10] J. D. Murray, *Mathematical Biology I: An Introduction*, In: Interdisciplinary Applied Mathematics, Vol. 18, Springer New York, 2002.
[11] J. D. Murray, *Mathematical Biology II: Spatial Models and Biomedical Applications*, In: Interdisciplinary Applied Mathematics, Vol. 18, Springer New York, 2003.
[12] K. J. Painter and T. Hillen, Volume-filling and quorum-sensing in models for chemosensitive movement, *Canadian Applied Mathematics Quarterly*, **10** (2002), 501–543.
[13] H. L. Smith, *Monotone Dynamical Systems: An Introduction to the Theory of Competitive and Cooperative Systems*, Mathematical Surveys and Monographs, 41. American Mathematical Society, Providence, RI, 1995.
[14] M. Winkler, Absence of collapse in a parabolic chemotaxis system with signal dependent sensivity, *Math. Nachr.*, **283** (2010), 1664–1673.
[15] D. Wodarz, *Killer Cell Dynamics: Mathematical and Computational Approaches to Immunology*, Interdisciplinary Applied Mathematics, vol. 32, Springer Berlin, 2007.
[16] D. Wrzosek, Global attractor for a chemotaxis model with prevention of overcrowding, *Nonlinear Analysis*, **59** (2004), 1293–1310.
[17] D. Wrzosek, Volume filling effect in modeling chemotaxis, *Math. Model. Nat. Phenom.*, **5** (2010), 123–147.
[18] F. Vianello, I. T. Olszak and M. C. Poznansky, Fugetaxis: Active movement of leukocytes away from a chemokinetic agent, *J. Mol. Med.*, **83** (2005), 752–763.
[19] P. Yu, Closed-form conditions of bifurcation points for general differential equations, *Int. J. Bifurcation Chaos Appl. Sci. Eng.*, **15** (2005), 1467–1483.

Received October 2015; revised December 2015.

E-mail address: xiulanlai@ruc.edu.cn
E-mail address: xzou@uwo.ca